Detection of Two Glass Transitions on Triton X-100 under Confinement

ARTICLE *in* THE JOURNAL OF PHYSICAL CHEMISTRY C · OCTOBER 2013

Impact Factor: 4.77 · DOI: 10.1021/jp404306a

THE JOURNAL OF PHYSICAL CHEMISTRY C

Article

pubs.acs.org/JPCC

Detection of Two Glass Transitions on Triton X-100 under Confinement

Esther G. Merino,[†] Paulo D. Neves,[†,‡] Isabel M. Fonseca,[†] Florence Danéde,[§] Abdenacer Idrissi,[∥] C. J. Dias,[‡] Madalena Dionísio,*[,†] and Natália T. Correia*[,†,§]

[†]REQUIMTE/CQFB, Departamento de Química, Faculdade de Ciências e Tecnologia, Universidade Nova de Lisboa, 2829-516 Caparica, Portugal

[‡]CENIMAT/I3N, Departamento de Ciência dos Materiais, Faculdade de Ciências e Tecnologia, FCT, Universidade Nova de Lisboa, 2829-516 Caparica, Portugal

[§]Unité Matériaux Et Transformations (UMET), UMR CNRS 8207, UFR de Physique, BAT P5, Université Lille Nord de France, F-59655 Villeneuve d'Ascq Cedex, France

[∥]Laboratoire de Spectrochimie Infrarouge et Raman (LASIR), UMR CNRS 8516, BAT C5, Université Lille Nord de France, F-59655 Villeneuve d'Ascq Cedex, France

ABSTRACT: Because of the strong tendency of Triton X-100 to crystallize, inclusion in a SBA-15 matrix of 5.7 nm in pore diameter was used as a means to suppress crystallization. Clear evidence that Triton X-100 exists under confinement in the amorphous and supercooled state is given by X-ray diffraction supported by differential scanning calorimetry and dielectric relaxation spectroscopy. From the thermogravimetric analysis, a loading degree of 50% (wt) was estimated; the decomposition of confined Triton X-100 follows a two-step profile, indicating that molecules are partitioned between bulklike and adsorbed, the latter fraction being in a higher proportion. This allowed the unequivocal detection by DSC of two well-resolved glass transitions (~20 K apart), which is a remarkable result obtained by conventional calorimetric analysis in confined systems. The two molecular populations have different mobilities giving rise to two different dielectric relaxation processes: an $\alpha_{Tr/SBA}$ bulklike process associated with molecules located more in the center of the pores, slightly slowed down relative to bulk α-relaxation, and an S-process due to molecules absorbed at the walls with significantly hindered mobility. Moreover, an MWS process is detected due to interfacial polarization that builds up between the adsorbed Triton X-100 molecules and SBA pore walls whose temperature dependence seems to be correlated with the one of the S-process. The inclusion in SBA-15 revealed to be a good strategy to simultaneously avoid crystallization and achieve a long-term stabilization of the disordered form.

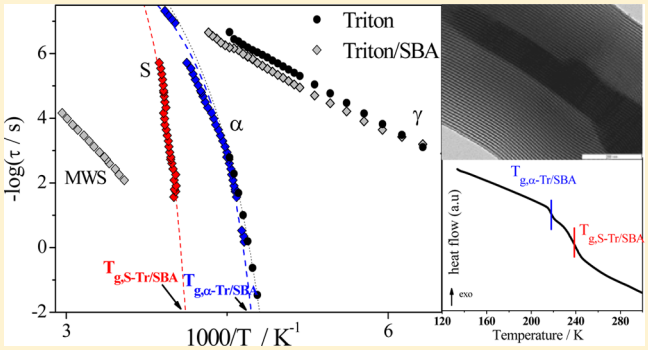

1. INTRODUCTION

Confinement studies emerged recently as an attractive means to explore fundamental concepts concerning condensed matter physics. In this context, particular attention is given to the influence of confinement on the glass transition:[1,2] for polymer thin films, the studies concern mainly the thickness dependence of the glass transition temperature (T_g), whereas, for molecular guests confined to nanosized porous restricted geometries, the focus is given to the influence of the host pore dimensions (refs 1, 3, and 4, and references therein); recently, a correlation between the glass transition temperature and the interfacial free volume has been proposed.[5]

In systems exhibiting a distribution of the glass transition as multilayered polymer thin films, sophisticated techniques are needed, such as neutron reflectivity, to reveal multiple T_g's,[6,7] instead of thermal techniques as calorimetry. Even for glass formers confined to nanogeometries, which have been extensively studied in the literature, the calorimetric detection of two glass transitions is not trivial. A few examples are provided as polystyrene/*o*-terphenyl solutions in controlled pore glasses (CPGs),[8] salol in silica mesopores,[9] propylene glycol in CPG,[10] and acetaminophen in nanoporous Vycor glass.[11]

In the present work, evidence of a bimodal behavior concerning the glass transition of the water-soluble, liquid surfactant Triton X-100 entrapped in a nanoporous matrix is investigated by differential scanning calorimetry (DSC) and dielectric relaxation spectroscopy (DRS). These techniques were employed in previous works by some of us[12,13] to evaluate the temperature-driven phase transformations and dynamical

Received: May 1, 2013
Revised: September 18, 2013
Published: September 18, 2013

   dx.doi.org/10.1021/jp404306a | *J. Phys. Chem. C* 2013, 117, 21516−21528

behavior of bulk anhydrous Triton X-100. X-ray diffraction and polarized optical microscopy were used as complementary tools.

It was found that Triton X-100 (see chemical structure in Scheme 1), despite being a glass former ($T_g \sim 212$ K), shows a strong tendency to crystallize from both molten and glassy states.

Scheme 1. Chemical Structure of Triton X-100; $n \sim 9-10$

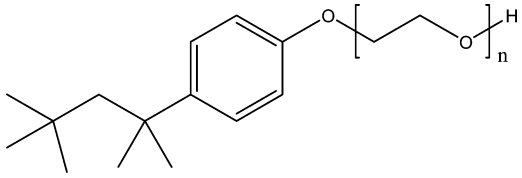

The dielectric spectra of bulk amorphous Triton X-100[13] evidence a multimodal character with several relaxation processes, which were designated as usual in an increasing order of frequency at which they are detected for a fixed T, as α, β, and γ. For the α-process, the usual curvature in the respective temperature dependence of relaxation times was found, from which a fragility index of 113 was estimated; the secondary β- and γ-processes exhibit linearity in the activation plot whose origin was attributed to localized motions: the activation parameters for the γ-process are comparable with the parameters of the corresponding process observed for the n-ethylene glycol dimethacrylate monomers ($1 \leq n \leq 4$),[14] allowing assigning it to dipolar fluctuations within the ethylene glycol moiety.[15] A higher length scale was assigned to the mechanism of the β-process, probably associated with hindered rotations of the octylphenyl ether group. Nevertheless, even avoiding crystallization on cooling, dielectric data obtained from the isothermal measurements carried out upon heating are sooner or later affected by cold crystallization being desirable to find a strategy to circumvent crystallization.

Motivated by the recent knowledge that molecular mobility and phase transformations can be significantly altered when a glass-forming liquid is confined into the nanometer scale, in the present work, Triton X-100 was included in a mesoporous silica matrix (SBA-15) with a pore size of 5.7 nm to evaluate the effect on its molecular dynamics and phase transformations.

Nanoconfinement emerged in the past few years as a strategy to stabilize otherwise metastable or transient polymorphs, as demonstrated for acetaminophen inside controlled pore glasses (CPGs).[16,17]

The production of a usable amorphous material implies the stabilization of a highly disordered state that can be also achieved by confining in nanoscaled geometries. In certain geometrical confinements, the guest molecules are unable to form a crystalline structure, and therefore, nanoconfinement is also a strategy to avoid crystallization.[11,18,19] The spontaneous amorphization of solid drugs by using mesoporous magnesium aluminum silicate was reported since 1986.[20] In the 1990s, the amorphization of lead when confined to carbon nanotubes was observed by Ajayan and Iijima,[21] which was rationalized by Prasad and Lele[22] as the pore size being smaller than the critical nucleus size.

The avoidance of crystallization gives origin to a supercooled liquid or glass, depending on the glass transition of the thus obtained state for the confined guest. The former can have an enhanced mobility compared with bulk, the acceleration in the dynamics being rationalized as an effect of the interference of the pore dimension with the characteristic length for the dynamic glass transition. This effect decreases the glass transition temperature, and could even suppress it, prolonging the supercooled state of the confined guest with enhanced mobility.[3,23−25] However, for rather low pore sizes, the guest molecules can undergo specific interactions with the pore wall, as has been shown for systems forming hydrogen bonds between the guest molecules and the inner pore, and the molecular dynamics can slow down.[3,26] Therefore, the dynamics of molecules confined to nanoporous hosts is controlled by a counterbalance between confinement and surface effects.[3,27] This behavior was shown by some of us by means of dielectric relaxation spectroscopy for the confined ibuprofen drug:[28] two families of molecules with different molecular mobilities were observed, one due to molecules close to the pores' center with a higher mobility compared to the bulk at low temperatures, and another with slower mobility that originated from molecules interacting with the pore walls (sketched in Figure 8 of ref 27). The same type of effect was also observed for other low-molecular-weight guests as salol in CPG,[29] and a nematic liquid crystal confined to mesopores,[30] as detected by dielectric spectroscopy; solid-state NMR studies also suggest the existence of two families of molecules for ibuprofen[31] and pyridine[32] confined to mesoporous silica.

In our previous studies, mesoporous silica-based materials were used as host systems as in the present work. These matrixes attract great interest due to their particular physical properties, such as ordered pore network, high internal surface area, silanol-containing surface, and chemical and mechanical stability.[33]

A full characterization of the physical state, dynamics, and physical stability of Triton X-100 entrapped in SBA-15 by DRS and DSC, X-ray diffraction, FTIR, and thermogravimetry is given in the present paper.

2. EXPERIMENTAL SECTION

Materials. Triton X-100, polyethylene glycol *tert*-octylphenyl ether, $C_{14}H_{22}O(C_2H_4O)_n$ with an average number, $n \sim 9-10$, of oxyethylene units per molecule (MW ~ 625) (see Scheme 1), was reagent grade purchased from Fluka (catalogue number 93420; CAS number: 9002-93-1). Hereafter, it will be designated as Triton.

A Karl Fisher analysis showed a water content of 0.28% (w/w). It was used without further purification.

Synthesis of SBA-15 and Triton Loading. SBA-15 (100% Si) used here as the mesoporous host was synthesized according to Gao et al.[34] employing the triblock copolymer, Pluronic P123, as template and tetraethoxysilane (TEOS) as silica source. Briefly, 2.0 g of Pluronic P123 was dissolved in 60 mL of 2 M aqueous HCl and 15 mL of distilled water under stirring. After homogenization, 4.4 g of TEOS was added dropwise to the solution at room temperature. The final mixture was stirred at 313 K for 24 h, transferred into a Teflon bottle sealed in an autoclave, and heated to 373 K for another 24 h. Finally, the resulting precipitate was filtered, washed carefully with distilled water, and air-dried. It was further calcinated at 773 K for 5 h to remove the template and impurities.

The textural characterization of the SBA-15 was based on the nitrogen adsorption isotherm, determined at 77 K with a Micromeritics ASAP 2010 apparatus. The average pore size and the pore size distribution was determined by the method of

dx.doi.org/10.1021/jp404306a | J. Phys. Chem. C 2013, 117, 21516−21528

Barrett–Joyner–Halenda (BJH),[35] in the desorption branch. The BJH method was originally designed for relatively wide-pore adsorbents with a wide pore size distribution.

However, it was repeatedly demonstrated that it can be successfully applied to virtually all types of porous materials. The model is based on the assumption that pores have a cylindrical shape and that pore radius is equal to the sum of the Kelvin radius and the thickness of the film adsorbed on the pore wall. The desorption branch of the isotherm in the pressure range ($0.4 < p/p_0 < 0.967$) is generally used as initial data for BJH calculations. BJH desorption analysis allowed estimating an average pore diameter of 5.7 nm (see pore width distribution in Figure 1). Furthermore, to obtain structural

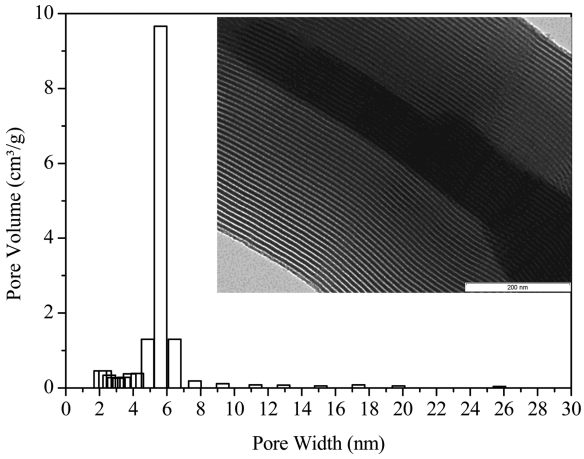

Figure 1. Pore width distribution of SBA-15 as determined by the BJH method; the inset shows a micrograph obtained by TEM (scale bar is 200 nm).

information at nanometer scale, transmission electron microscopy (TEM) analysis was carried in a JEOL-JEM-2010 electronic transmission microscope, confirming the uniform structure of two-dimensional hexagonally ordered cylindrical pores (inset of Figure 1).

Specific area, 822 $m^2 \cdot g^{-1}$, and pore volume, 0.924 $cm^3 \cdot g^{-1}$, were estimated from the BET method. For the loading, SBA-15 was previously finely grounded and left for 6 h at 10^{-4} mbar and 393 K to remove water. A Triton solution in ethanol (~3% (v/v)) was added to 0.1 g of the dried SBA-15 powder and kept for 24 h under gentle stirring; afterward, the suspension was left at rest overnight at room temperature, leading to complete evaporation of solvent. The excess of nonconfined Triton was removed by washing with a small amount of ethanol, and the solvent removal was assured by vacuum drying at 353 K for 6 h. The unloaded matrix will be designated as SBA and the composite as Triton/SBA. The unloaded SBA was submitted to a protocol similar to the one used for the loading using only ethanol, in order to compare with the loaded matrix. Samples were handled in a desiccator.

Attenuated Total Reflectance-Fourier Transform Infrared (ATR-FTIR) Spectroscopy. Fourier transform infrared (FTIR) spectra over the range of 350–4000 cm^{-1} were collected at room temperature using a Bruker Tensor 27 FT-IR spectrometer equipped with a Pike Miracle single-bounce attenuated total reflectance (ATR) cell with a ZnSe single crystal, with a DTGS detector and a KBr beam splitter. All the spectra were recorded via the ATR method with a resolution of 2 cm^{-1} and 60 scans.

Thermogravimetric Analysis (TGA). The thermogravimetric measurements were carried out with a TGA 7 apparatus from PerkinElmer under a highly pure nitrogen atmosphere with a flow rate of 20 $mL \cdot min^{-1}$. The temperature reading was calibrated using the Curie points of alumel and nickel standards, while the mass reading was calibrated using balance tare weights provided by PerkinElmer.

In this work, the weight loss due to the burning and decomposition of the organic molecules is detected up to ca. 800 K while the SBA matrixes are thermally stable up to temperatures above 1000 K (its weight is constant by increasing the temperature up to 1073 K).

X-ray Diffraction. X-ray diffraction analysis was carried out with a diffractometer using Cu Kα radiation (selected wavelength $\lambda_{Cu\ K\alpha 1}$ = 1.54056 Å) in the 2θ range of 0.2–113.8° (2θ step 0.015°). The powder X-ray diffraction patterns were recorded in real time with an INEL curved position-sensitive detector (CPS 120) giving simultaneous detection over 120°. The samples were enclosed in a Lindemann glass capillary (diameter = 0.7 mm) mounted on the axis of a G3000 goniometer (see ref 36 for more details). A Cryostream Plus controller from Oxford Cryosystems was used to regulate the temperature. X-ray diffraction patterns of bulk Triton, unloaded SBA, and Triton/SBA were first collected at room temperature during a total counting time of 15 h. Additionally, X-ray diffraction patterns for the three materials were isothermally collected by ranging the temperature from 173 to 293 K (for bulk Triton, X-ray patterns were collected every 5 K and, for the other samples, every 10 K); total counting time at each scanned temperature was of 600 s for bulk Triton and 900 s for both the unloaded SBA matrix and the Triton/SBA composite.

Differential Scanning Calorimetry (DSC). The calorimetric experiments were carried out with a DSC Q2000 from TA Instruments Inc. (Tzero DSC technology) operating in the Heat Flow T4P option (details can be found in ref 37); scans at cooling and heating rates of 30 $K \cdot min^{-1}$ were performed, covering the temperature range from 123 to 383 K. The high heating rate was used in order to increase the sensitivity of the calorimetric signal to enhance the heat capacity jumps associated with the glass transitions of Triton confined to SBA mesopores; the unloaded SBA matrix and bulk Triton X-100 were also calorimetrically measured under the same conditions.

Measurements were realized under dry high-purity helium at a flow rate of 50 $mL \cdot min^{-1}$; a liquid nitrogen cooling system (LNCS) was used in order to reach temperatures as low as 123 K. DSC Tzero calibration was carried out in the temperature range from 108 to 573 K. It requires two experiments: the first run with the empty cell (baseline) and the second run with equal weight sapphire disks on the sample and reference platforms (without pans). This procedure allows for cell resistance and capacitance calibration, which compensates for subtle differences in thermal resistance and capacitance between the reference and sample platforms in the DSC sensor. Enthalpy (cell constant) and temperature calibration were based on the melting peak of the indium standard (T_m = 429.75 K) supplied by TA Instruments (lot # E10W029). Small amounts of samples (less than 5 mg) were encapsulated in Tzero (aluminum) hermetic pans with a Tzero hermetic lid with a pinhole; when a standard pan (open) is used, the endotherm due to water removal (in the unloaded SBA matrix and Triton/SBA samples) persists even after running several scans up to 373 K.

dx.doi.org/10.1021/jp404306a | J. Phys. Chem. C 2013, 117, 21516–21528

Dielectric Relaxation Spectroscopy (DRS). Dielectric measurements were carried out using the ALPHA-N impedance analyzer from Novocontrol Technologies GmbH, covering a frequency range from 10^{-1} Hz to 1 MHz. A small amount of Triton/SBA was slightly compressed between two gold-plated electrodes (10 mm in diameter) of a parallel plate capacitor, BDS 1200 with two silica spacers, 50 μm in thickness. The sample cell was mounted on a cryostat, BDS 1100, and exposed to a heated gas stream being evaporated from a liquid nitrogen Dewar. The temperature control is assured by the Quatro Cryosystem and performed within ±0.5 K. Novocontrol Technologies GmbH supplied all of these modules. After a previous cooling ramp at 11 K·min^{-1} from room temperature to 153 K, isothermal dielectric spectra were collected between 153 and 393 K at different increasing temperature steps: from 195 to 273 K in steps of 2 K and, in the remaining temperature range, every 5 K.

Several cooling and heating ramps were carried out at different rates (11, 4, and 2 K·min^{-1}) to evaluate the physical state of the confined guest and the influence of thermal history in its phase transformations. The complex dielectric permittivity was measured in isochronal mode, $\varepsilon^*(T)$, at five frequencies sufficiently high to allow a reliable measurement (100, 1×10^3, 1×10^4, 1×10^5, 1×10^6 Hz) during the heating/cooling cycles, in the temperature range between 153 and 393 K.

Dielectric Data Analysis. To analyze the isothermal dielectric data, the model function introduced by Havriliak–Negami was fitted to both imaginary and real components of complex permittivity. Because multiple peaks are observed in the available frequency window, a sum of HN-functions was employed:

$$\varepsilon^*(f) = \varepsilon_\infty + \sum_j \frac{\Delta\varepsilon_j}{[1 + (i\omega\tau_{\mathrm{HN}\,j})^{\alpha_{\mathrm{HN}\,j}}]^{\beta_{\mathrm{HN}\,j}}} \quad (1)$$

where j is the index over which the relaxation processes are summed, $\Delta\varepsilon$ is the dielectric strength, τ_{HN} is the characteristic HN relaxation time, and α_{HN} and β_{HN} are fractional parameters ($0 < \alpha_{\mathrm{HN}} < 1$ and $0 < \alpha_{\mathrm{HN}}\cdot\beta_{\mathrm{HN}} < 1$) describing, respectively, the symmetric and asymmetric broadening of the complex dielectric function.[38] From the estimated values of τ_{HN}, α_{HN}, and β_{HN} parameters, a model-independent relaxation time, $\tau = 1/(2\pi f_{\max})$, was calculated according to[38−40]

$$\tau = \tau_{\mathrm{HN}} \times \left[\frac{\sin\left(\frac{\alpha_{\mathrm{HN}}\beta_{\mathrm{HN}}\pi}{2+2\beta_{\mathrm{HN}}}\right)}{\sin\left(\frac{\alpha_{\mathrm{HN}}\pi}{2+2\beta_{\mathrm{HN}}}\right)}\right]^{1/a_{\mathrm{HN}}} \quad (2)$$

Close to the glass transition temperature, the temperature dependence can be described by the well-known Vogel/Fulcher/Tammann/Hesse equation,[41−43] which reads

$$\tau(T) = \tau_\infty \exp\left(\frac{B}{T - T_0}\right) \quad (3)$$

where τ_∞ and B are constants and T_0 is the so-called Vogel temperature.

3. RESULTS AND DISCUSSION

Evidence of Inclusion of Triton into Nanopores. Triton was entrapped in the SBA nanoporous matrix, with an average pore diameter of 5.7 nm (see the Experimental Section). To evaluate if a successful loading was achieved, ATR-FTIR was used. The spectra thus collected are compared in Figure 2 for unloaded (SBA) and loaded (Triton/SBA) matrix, and bulk Triton.

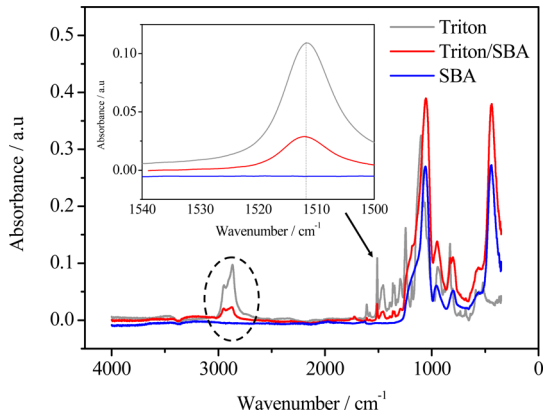

Figure 2. ATR-FTIR spectra of Triton/SBA compared with bulk Triton and unloaded SBA at room temperature. The inset presents the ATR-FTIR spectra in the frequency region of C−C stretching. The dashed curve in the main graph indicates the region of the spectrum due to the C−H stretch.

Two main regions give the evidence of a successful loading: (i) one at a wavenumber of 1512 cm^{-1} assigned to a coupling of aromatic ring C−C stretching and C−H deformation modes in Triton[44] (see a scale-up in the inset) and (ii) a band near 3000 cm^{-1} due to C−H stretch (dashed circle). These two absorptions are absent in the spectrum of the unloaded matrix. The more intense band in the Triton spectrum is due to the C−O−C vibration of the oligomeric poly(oxyethylene) chain, which appears[45] near 1100 cm^{-1} partially overlapping the Si−O−Si bend of SBA detected at slightly lower wave numbers.[46]

To quantify the amount of loaded Triton into SBA, thermogravimetric analysis was carried out; see Figure 3. From the weight loss due to the burning and decomposition of the guest molecules, measured up to ca. 1073 K, the Triton loading degree was estimated as ∼50% (wt). It is important to note that the decomposition onset in a derivative plot (mg·

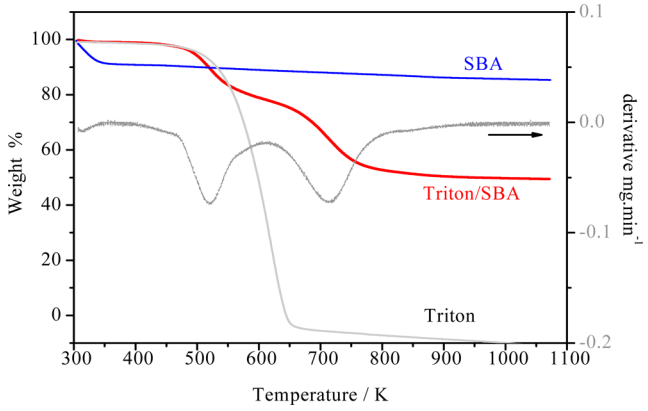

Figure 3. Thermogravimetric curves obtained on heating at 10 K·min^{-1} for SBA unloaded and loaded with Triton (Triton/SBA) and for bulk Triton. The derivative plot for Triton/SBA is included (right-hand vertical axis) evidencing the two peaks corresponding to the two-step weight loss decomposition of the composite.

dx.doi.org/10.1021/jp404306a | J. Phys. Chem. C 2013, 117, 21516−21528

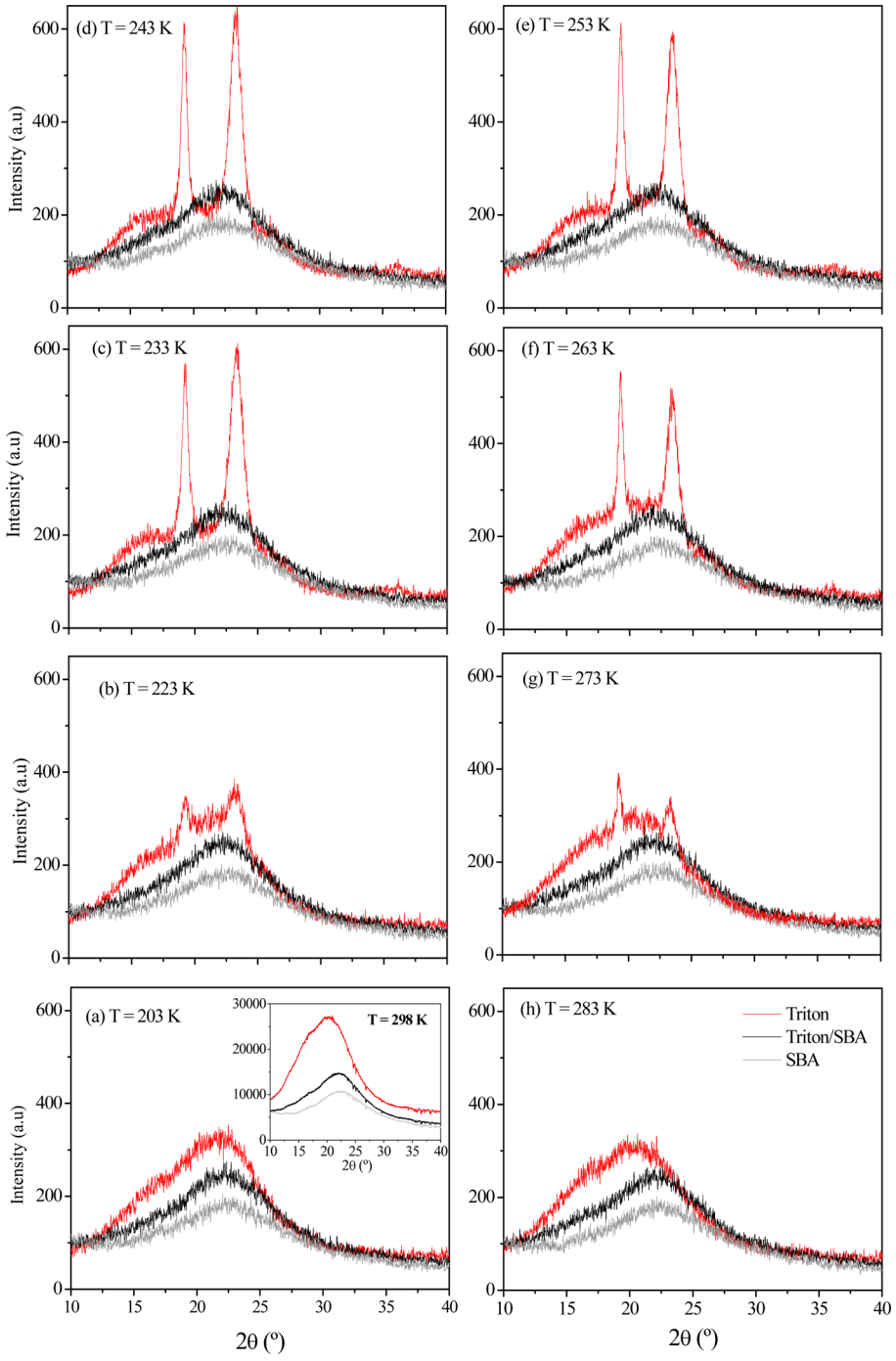

Figure 4. Temperature evolution of the X-ray diffraction patterns for bulk Triton (red, upper curves), unloaded SBA (gray, bottom curves), and Triton/SBA (black, middle curves) obtained upon heating after an initial quenching to 173 K. The progress of Bragg peaks in (a)−(d) illustrates cold crystallization and in (e)−(h) the respective melting of bulk Triton; confined Triton always exhibits the halo characteristic of the amorphous form. The inset in graph (a) shows the initial pattern for the three systems at room temperature (see details in the Experimental Section).

min^{-1}) is mass-independent as found for Triton (not shown). However, in the wt % thermogram (scanned at 10 $K{\cdot}min^{-1}$), an apparent mass dependence is observed; for this reason, the thermogram included in Figure 3 is the one obtained for a sample with ∼0.5 mg, which compares to the Triton mass loaded in the SBA matrix taking into account the loading degree.

Contrary to the neat guest that decomposes in a single weight loss, the composite decomposes in a two-step weight loss, which is supported by the derivative curve that exhibits two peaks, the second one having a greater area than the one that shows up at lower temperatures; this will be commented on further on. It was observed that the mesoporous matrix is thermally stable up to temperatures above 1000 K (after a small initial weight loss due to water/solvent removal, its weight is constant by increasing the temperature up to 1073 K). In the loaded matrix, the initial drop due to water/solvent evaporation is negligible (<1% (wt)).

The two analyses, FTIR and TGA, give an indication that a successful loading of Triton was achieved.

dx.doi.org/10.1021/jp404306a | J. Phys. Chem. C 2013, 117, 21516−21528

Characterization of Triton/SBA. To access the physical state, X-ray diffraction and differential scanning calorimetry were used. Furthermore, the molecular mobility of Triton confined in SBA was probed by dielectric relaxation spectroscopy. The analysis by these different techniques is described next.

X-ray Diffraction. Figure 4 presents the powder X-ray diffraction patterns of bulk Triton, unloaded SBA matrix, and Triton/SBA composite at some representative temperatures taken upon heating after a quenching from room temperature to 173 K. The initial state of all materials, at room temperature, is shown in the inset of Figure 4a. In this first pattern, the three materials present the halo characteristic of the amorphous form with no observable Bragg peaks. The Bragg peaks typical of the long-range order of the two-dimensional hexagonal symmetry of the SBA mesoporous matrix are only visible at small angles, $2\theta < 10°$ (for details, see ref 46).

For the lower temperatures (Figure 4a at 203 K), bulk and confined Triton exhibit a diffraction pattern similar to the one taken at room temperature, confirming that both are still amorphous after the initial quenching. With the temperature increase, bulk Triton undergoes cold crystallization, as seen by the emergence of two Bragg peaks that become more intense up to 243 K, but an amorphous halo is still present (Figure 4, from a to d). This means that, at these temperatures, bulk Triton is semicrystalline. With further heating (Figure 4e–h), the Bragg peaks become depleted due to melting, however, gradually extending over a relatively wide temperature range (~30 K). Concerning the confined material, it kept the same diffraction pattern, characteristic of the amorphous form, at all temperatures despite being submitted to the same thermal treatment as the bulk material. Therefore, it can be concluded that confined Triton is amorphous, persisting in this form and, therefore, not undergoing any phase transformation under the applied thermal treatment.

Differential Scanning Calorimetry. DSC measurements were carried out for confined and bulk Triton, and for the unloaded matrix. The respective thermograms taken in the first and second heating scans (see the Experimental Section) are shown in Figure 5. In the first scan (gray solid lines), a broad endothermic peak with onset temperature above 273 K is observed in the thermograms originated by water evaporation mainly for unloaded SBA (Figure 5a), in agreement with the TGA analysis. For bulk Triton, the thermogram (Figure 5c) is dominated by the exothermal peak due to cold crystallization, immediately followed by the endotherm caused by melting; at lower temperatures, the heat flow jump due to the glass transition is also present. Interesting enough is the two-step profile exhibited by the heat flow for confined Triton and the absence of any exotherm/endotherm due to crystallization/melting (Figure 5b,c).

In the second scan (black solid lines) taken for the dried materials, no thermal event is detected for the unloaded SBA as expected. Bulk Triton still exhibits the heat flow jump taken as the glass transition signature. In the present conditions, the onset and midpoint temperatures (see Table 1) are in good agreement with the values previously reported at different cooling and heating rates.[12,13] A crystallization exotherm is observed at ~238 K, despite the high heating rate (30 K·min^{-1}). The endotherm due to melting extends over a relatively wide temperature range ($\Delta T \approx 33$ K), in agreement with the melting monitored by X-ray diffraction and the calorimetric behavior reported previously under different conditions.[12,13]

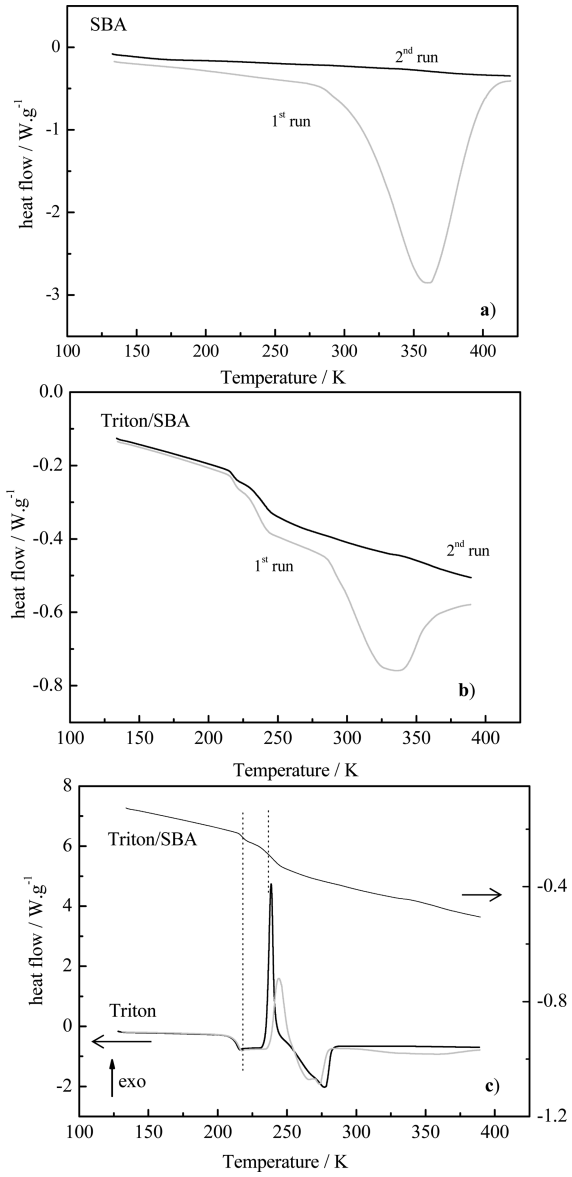

Figure 5. Thermograms (heat flow vs temperature) collected on heating at 30 K·min^{-1} of (a) unloaded SBA matrix (m = 2.30 mg), (b) confined Triton in SBA ($m_{Triton+SBA}$ = 2.47 mg), and (c) compared with bulk Triton (m = 3.33 mg): 1st heating scan (gray solid lines), 2nd scan (black solid lines).

The thermogram for the confined system, Triton/SBA, still does not exhibit either crystallization or melting. This means that the guest did not undergo crystallization either during inclusion or upon the calorimetric thermal treatment. Moreover, it confirms that bulk Triton outside the pores was efficiently removed during the washing step, otherwise, given its high ability to undergo crystallization, it would originate a bulklike melting transition observable by DSC as found for other composites.[47,48]

The crystallization suppression, which is reproducible in subsequent runs, is coherent with the observations from X-ray diffraction. Moreover, as mentioned before for the first scan, for confined Triton, the heat flux evolves according to a two-step profile. The one located at lower temperatures is quite close to the one observed for bulk Triton (Figure 5c), and thus, it is originated by the glass transition of bulklike Triton molecules in the composite (named here as process I). This result is a

dx.doi.org/10.1021/jp404306a | J. Phys. Chem. C 2013, 117, 21516–21528

Table 1. Summary of the Calorimetric Data for the Confined System, Triton/SBA, Unannealed and after Annealing at 213 and 223 K[a]

	bulk Triton	Triton/SBA					
		unannealed		annealed at 213 K		annealed at 223 K	
	unannealed	I	II	I	II	I	II
$T_{g,onset}$/K	210.5	215.5	232.5	216.8	233.9	216.2	230.4
$T_{g,midpoint}$/K	214.3	217.9	240.0	219.2	238.9	218.9	234.9
ΔC_p/J·g^{-1}·K^{-1}	0.886	0.530		0.526		0.530	

[a]Glass transition onset ($T_{g,onset}$) and midpoint ($T_{g,midpoint}$) for the two glass transitions identified as I and II; heat capacity jump is the total ΔC_p associated with the two transitions observed on heating (see details in text).

further confirmation that Triton exists under confinement as an amorphous material. The second step in the heat flow for the Triton/SBA composite has a midpoint located at 240 K (process II), having a higher heat flow jump than process I; this result can be taken as an indication that more Triton molecules contribute to the second glass transition process. Both midpoint and onset values of the two glass transition temperatures ($T_{g,midpoint}$, $T_{g,onset}$) for processes I and II are reported in Table 1, including the calorimetric data for bulk Triton.

After annealing during 1 h at 213 K ($T_{g,on\ I}$ − 2.5 K) and at 223 K ($T_{g,on\ II}$ − 9.5 K) (see the Experimental Section), the heat flow jumps I and II became enhanced: Figure 6 presents

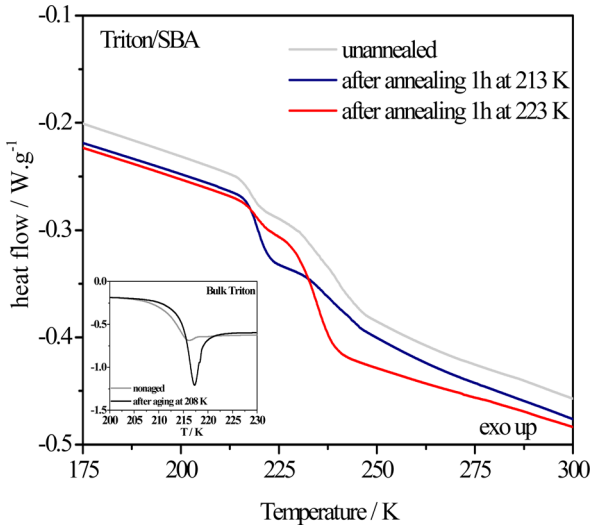

Figure 6. Scale-up of the thermograms in the glass transition region obtained for confined Triton (Triton/SBA) unannealed and after 1 h annealing at the indicated temperatures, enhancing the two-step profile ($m_{Triton+SBA}$ = 2.47 mg; loading degree 50% (wt)); the thermogram of bulk Triton (m = 3.33 mg) is included in the inset for comparison concerning the annealing/aging effect.

the thermograms obtained after annealing at 213 K (blue solid line) and 223 K (red solid line). The values of the heat capacity, ΔC_p, estimated for unannealed and annealed Triton/SBA are presented in Table 1 after normalization for the loading degree (50% (wt)). Prior to normalization, the ΔC_p values were estimated as the height of the heat flow in the two-step region (Figure 6) between the tangent to the final baseline taken at a temperature well above the value of $T_{g,II}$, 325 K, and the tangent to the initial slope taken at a temperature well below $T_{g,I}$, 163 K. This ΔC_p represents the total difference in the heat capacity between the confined equilibrium state and the confined out-of-equilibrium/glass Triton.

Bulk Triton was submitted also to annealing during 1 h at 208 K ($T_{g,on}$ − 2.5 K). The respective thermogram obtained after this thermal treatment is included in the inset of Figure 6, allowing a clear view of the enthalpy overshoot due to structural relaxation (physical aging). The absence of the enthalpy overshoot for confined Triton goes in line with the DSC findings reported for *ortho*-terphenyl confined to nanopores[49] and, more recently, for thin polymer films,[50] where the depression of the enthalpy overshoot is attributed to an acceleration of the physical aging process with the decrease of confining dimensions; we do not go further on this discussion since it is out of the scope of the present paper.

The unambiguous detection of two well-resolved heat flux discontinuities associated with the glass transitions of each family of different molecular mobility as found here for Triton confined to the SBA matrix is not so trivial under conventional DSC conditions. As mentioned previously in the Introduction, only a few identical examples are given in the literature for low-molecular-weight materials as for acetaminophen confined in Vycor glass where the two steps in DSC are occasionally found,[11] and propylene glycol in CPG,[10] for which the second step has a weak strength, contrary to what is observed in the present work for confined Triton.

To get a further insight in the dynamical behavior of the confined guest, dielectric relaxation spectroscopy was carried out, and results are described in the next section.

Dielectric Relaxation Spectroscopy. To further investigate the physical state of the entrapped Triton, the first dielectric measurements were performed by cooling the composite Triton/SBA from room temperature down to 153 K without any previous thermal treatment. Measurements were performed in ramp mode (5 frequencies) during cooling carried out at 11 K·min^{-1}, and stepwise upon heating by isothermally collecting the dielectric spectra over a large frequency range (see the Experimental Section).

These conditions are identical to the ones used for bulk Triton[13] in order to avoid the occurrence of melt crystallization. Figure 7a compares the real permittivity temperature dependence for confined Triton with the bulk material. The step in the $\varepsilon'(T)$ trace detected in both cooling scans (down arrows) is characteristic of the glass transition that is also observed on the further heating scan obtained from isothermal measurements for Triton/SBA. Figure 7a includes the $\varepsilon'(T)$ trace obtained from heating at 9 K·min^{-1} for bulk Triton for comparison, which exhibits the typical signature of cold crystallization, that is, a frequency-independent drop at around 225 K.[12] This event is absent in the $\varepsilon'(T)$ trace of Triton/SBA, despite being collected at a much slower heating rate; the average heating rate

dx.doi.org/10.1021/jp404306a | J. Phys. Chem. C 2013, 117, 21516−21528

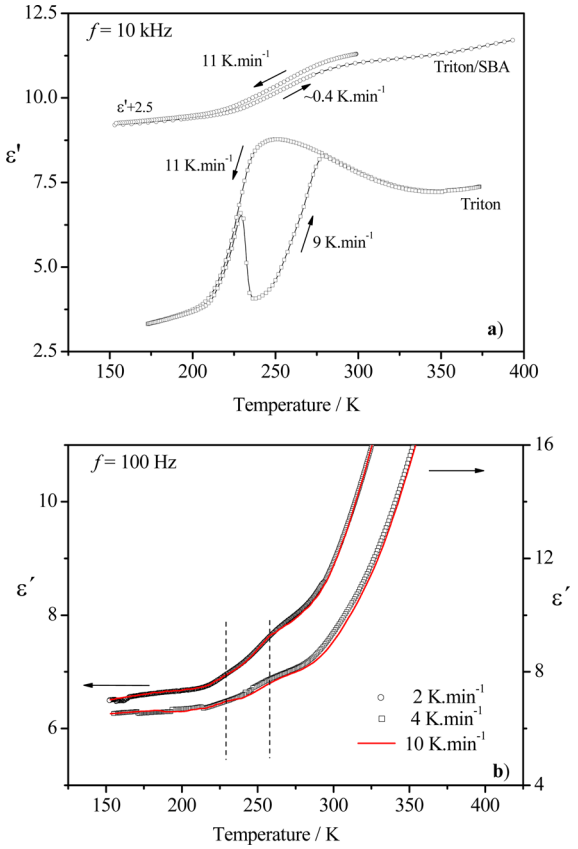

Figure 7. (a) Temperature dependence of the real part of the complex dielectric function ($\varepsilon'(T)$) for Triton/SBA and bulk Triton. The $\varepsilon'(T)$ trace for the bulk material[12] illustrates the typical profile when cold crystallization occurs by the drop in this property (here, observed at ~225 K) absent for Triton/SBA. Run_1 (down arrows): $\varepsilon'(T)$ measured during a cooling ramp at 11 K·min^{-1} for both Triton and Triton/SBA. Run_2 (up arrows): $\varepsilon'(T)$ measured on heating at 9 K·min^{-1} for bulk Triton and taken from isothermal measurements for confined Triton/SBA (~0.4 K·min^{-1}). For a better clarity, the $\varepsilon'(T)$ values for the confined system were vertically shifted by adding 2.5. (b) $\varepsilon'(T)$ traces for Triton/SBA taken at 2 and 4 K·min^{-1} cooling rates (symbols) and further heating at 10 K·min^{-1} (solid red lines) showing a two-step-like glass transition profile (dashed lines are only indicative of the temperature location of each step); the ε' increase at high temperatures is due to an MWS process.

upon isothermal measurements performed between 193 and 273 K is around 0.4 K·min^{-1}. The obtained $\varepsilon'(T)$ trace ends without any discontinuity, meaning that either no cold crystallization or no melting of any previously formed crystalline phase occurred, confirming the DSC and X-ray results. Therefore, further evidence is being provided by dielectric spectroscopy that Triton exists in the amorphous state when confined in the SBA matrix (5.7 nm in pore size).

To evaluate the stability of the amorphous state for the confined guest, different temperature scans were run at relatively low cooling rates: 4 and 2 K·min^{-1}, which are included in Figure 7b. Whereas bulk Triton crystallizes during measurements at a low cooling rate (and/or heating rate),[12] for the confined guest, crystallization was never observed, as seen by the absence of the typical sudden drop in ε'. This behavior is reproducible, confirming that the confinement of Triton into an SBA matrix is a good strategy to avoid crystallization. It should be noted that the aging studies by DSC (Figure 6) and the ramp dielectric experiments carried out at 2 and 4 K·min^{-1} were performed by the time of the redaction of this paper with the sample being prepared 24 months ago, confirming that Triton inside the mesoporous structure is still in the amorphous state.[51]

The high-temperature tail in the $\varepsilon'(T)$ trace shown in Figure 7b is due to a Maxwell/Wagner/Sillars[38] process originated by the coexistence of two different dielectric media: the Triton guest and the SBA matrix. The vertical dashed lines indicate a two-step glass-transition-like trace that agrees with the DSC thermograms and that will be discussed further on.

Isothermal DRS measurements were taken from 153 to 393 K for Triton/SBA after a previous heating up to 373.15 K. Figure 8 presents the isochronal plots taken from the isotherms

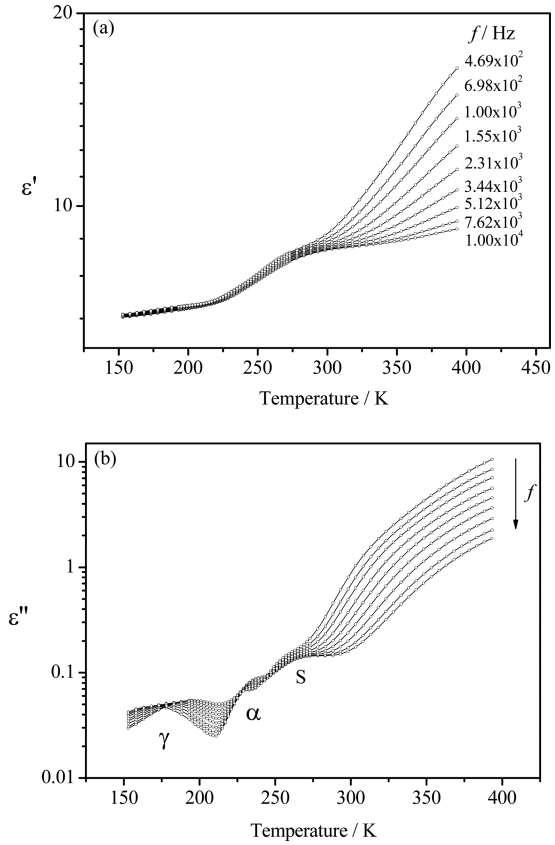

Figure 8. Temperature dependence of the complex permittivity (a) real, ε', and (b) imaginary, ε'', parts at some representative frequencies collected for Triton/SBA upon isothermal measurements; the arrow indicates the direction of increasing frequency.

of the real (a) and imaginary (b) parts of the complex permittivity at different frequencies; Figure 9 compares the behavior for Triton/SBA with the unloaded matrix SBA and bulk Triton at frequency f = 10 kHz.

It must be noted that the dielectric loss of the dried SBA matrix is negligibly small compared to that observed for the filled matrix (Figure 9); therefore, the detected dielectric response for the Triton/SBA composite is dominated by the response of Triton molecules.

A multimodal character for both $\varepsilon'(T)$ and $\varepsilon''(T)$ traces is found as already observed for bulk Triton (see the Introduction).[13] The comparison with bulk Triton allows assigning the detected processes: at the lowest temperatures, the results clearly show the presence of one secondary relaxation that is also detected in the bulk Triton, the γ-

dx.doi.org/10.1021/jp404306a | J. Phys. Chem. C 2013, 117, 21516−21528

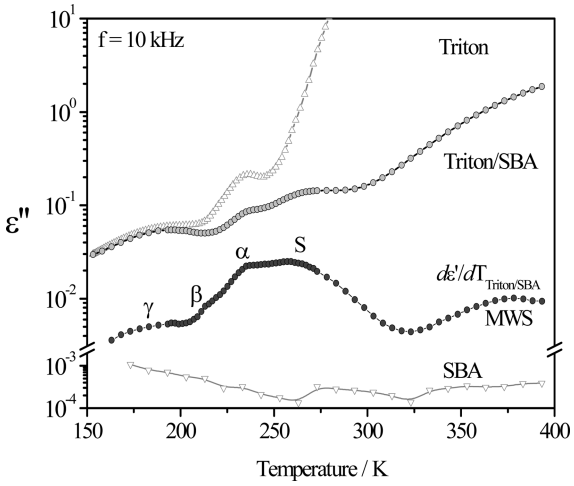

Figure 9. Dielectric loss (ε'') of confined Triton (Triton/SBA) vs temperature at a frequency of 10 kHz compared with bulk Triton and dried SBA matrix. The plot of ε' derivative enhances the multimodal profile of the isochronal $\varepsilon''(T)$ trace from which the maxima at different frequencies were taken to obtain the temperature dependence of relaxation times of $\alpha_{\text{Triton/SBA}}$-, S-, and MWS processes.

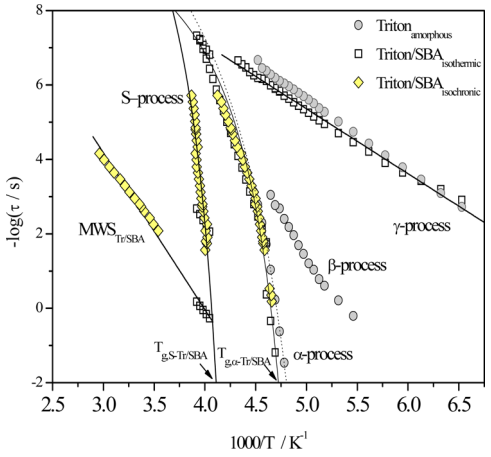

Figure 10. Relaxation map of all detected processes for the confined system Triton/SBA: squares represent the τ values estimated from the HN fit to the isothermal data and rhombi the τ values obtained from the Gaussian deconvolution of the isochronal plots; the relaxation times for the full amorphous (circles) Triton[13] are also included for comparison. The lines are fits of the Arrhenius and VFTH equations to the corresponding data of the confined system; the VFTH fit to the α-process of the amorphous bulk Triton is included as a dashed line.

process, followed by a bulklike α-relaxation. The comparison at different frequencies leads us to conclude that this latter process in the confined guest is slightly shifted to higher temperatures. This means that the molecular guest under confinement is slightly less mobile, which will be analyzed afterward.

In addition, two other processes are detected at lower frequencies (higher temperatures) relative to this bulklike α-process. A similar behavior was observed for other confined guests where, besides an interfacial polarization process at the highest temperatures (lowest frequencies), a new process emerges compared to the bulk material. This process is designated as surface process (S) and is attributed to guest molecules interacting with the pore surface of the host.[52−54]

The data analysis was extended to the isochronal representation of the dielectric loss, that is, ε'' versus temperature at constant frequencies ($\varepsilon''(T; f = \text{const})$). To investigate in detail the different relaxation processes for confined Triton, the isochronal representation of the dielectric loss, ε'', at a constant frequency versus temperature ($\varepsilon''(T; f = \text{const})$) is now analyzed. The dielectric loss can be described as a superposition of k Gaussians functions[55] and can be used to obtain the maximum temperature of peaks, T_{max}, for some of the frequencies measured. This method proved to be useful when the multiple relaxation processes present a very low response, making the analysis of dielectric loss spectra in the frequency domain very difficult.[28,55−57] The obtained T_{max} values were confirmed by the analysis of the peaks' position in the ε' derivative plot,[58] which is better resolved; the respective plot is included in Figure 9, allowing us to distinguish also, at the chosen frequency (10 kHz), the secondary $\beta_{\text{Triton/SBA}}$-process. At higher temperatures, the MWS process becomes clearly visible in the derivative of the isochronal plot from which the respective T_{max} values were obtained.

Figure 10 shows the temperature dependence of the relaxation time τ obtained from the isochronal plots ($\tau = 1/(2\pi f)$, $1/T_{max}$) for the $\alpha_{\text{Triton/SBA}}$-, S-, and MWS processes of confined Triton (yellow rhombi); the τ values for the MWS process were obtained from the derivative of the isochronal ε' plot. Because the $\gamma_{\text{Triton/SBA}}$-process emerges relatively well-defined, it was possible to fit the HN function (eq 1) to both $\varepsilon'(\omega)$ and $\varepsilon''(\omega)$ curves obtained from the isothermal measurements. The thus estimated relaxation times are included in the relaxation map together with the $\tau(T)$ values at some definite temperatures estimated for also the $\alpha_{\text{Triton/SBA}}$-, S-, and MWS processes. In the temperature ranges at which the relaxation times were estimated from both isothermic and isochronal data, a very good agreement is obtained, validating the analysis through the isochronal plots.

The relaxation map in Figure 10 also contains the temperature dependence of relaxation times for bulk amorphous Triton (light gray). The parameters obtained from the Arrhenius ($\tau(T) = \tau_\infty \exp(E_a/RT)$, where τ_∞ is the pre-exponential factor and E_a is the activation energy; R is the ideal gas constant and T the temperature) and VFTH fits to the temperature dependence of each relaxation process are presented in Table 2.

A close inspection of the activation plot evidences that a slightly different slope, and, consequently, a slightly different activation energy, is found for the secondary $\gamma_{\text{Triton/SBA}}$-process of confined Triton compared to bulk. While the loss curves of both amorphous Triton and Triton/SBA superimpose at the lowest temperatures—in frequency location, since the magnitude of the dielectric response is much lower for the composite—for temperatures higher than 173 K, the loss curves collected for Triton/SBA are shifted toward lower frequency compared with bulk amorphous, meaning that this relaxation mode in the confined guest becomes slightly less mobile; this gives rise to a slightly lower slope in the Arrhenius plot and thus a relatively inferior activation energy ($E_a = 33.4 \pm 0.4$ kJ·mol^{-1}).

The β-process was observed for bulk Triton, either amorphous or semicrystalline.[13] For the confined system, it is also felt in the isotherms and isochronal plots (see derivative plot in Figure 9), but no value is provided here in the relaxation map, since it is not possible to extract unequivocally the relaxation times from the raw data.

dx.doi.org/10.1021/jp404306a | J. Phys. Chem. C 2013, 117, 21516−21528

Table 2. Summary of the Activation Parameters (Arrhenius and VFTH (eq 3)) for All Detected Processes in the Different Conditions Investigated in the Present Work; the Fragility Index m Is Also Given

relaxation process	activation parameters	Triton amorphous[a]	Triton/SBA
α	τ_∞/s	1.0×10^{-14}	5.0×10^{-12}
	B/K	1080.2	587.8
	T_0/K	178.9	192.5
	T_g (τ = 100 s)/K	208.3	211.7
	m	113	147
β	E_a/kJ·mol	80 ± 3	not analyzed
	τ_∞/s	5.4×10^{-23}	
γ	E_a/kJ·mol^{-1}	36.3 ± 0.1	33.4 ± 0.4
	τ_∞/s	7.5×10^{-16}	8.4×10^{-15}
S[b]	τ_∞/s		7.0×10^{-15}
	B/K	not observed	669.6
	T_0/K		225.5
	T_g (τ = 100 s)/K		243.5
MWS[c]		not observed	τ_∞/s = 1.5×10^{-1}
			E_a/kJ·mol^{-1} = 81 ± 2

[a]The same designation as used in ref 13 is applied here. [b]The S-process is typical of the confined system, Triton/SBA. [c]The MWS process in confined Triton has Arrhenius temperature dependence.

Concerning the $\alpha_{Triton/SBA}$-process, its temperature dependence of relaxation times is curved versus the temperature reciprocal as characteristic of a cooperative process being described by a VFTH equation (eq 3) (solid line in Figure 10). With decreasing T, the relaxation times for confined Triton deviate from those of the bulk in such a way that they are higher at the same temperature, indicating that the dynamics associated with the glass transition is somewhat slower compared to that of the bulk. As a consequence, the glass transition temperature obtained for Triton/SBA from extrapolation of the VFTH equation to τ = 100 s[59,60] is $T_{g,100\ s}$ = 211.7 K, slightly higher than $T_{g,bulk}$ (see Table 2); the parameters of the VFTH equation were found by considering all the relaxation times, that is, thus obtained through either isothermal or isochronal plots. The 3.4 K increase of the glass transition temperature compared with bulk is in good agreement with the increase determined from DSC results (~4 K). These results are coherent with the observations reported by Schüler et al.[54] for propylene glycol and its oligomers that found a shift of 4.5 K toward higher temperatures for the glass transition of the confined material compared to that of the bulk being an example where geometrical restriction results in retardation of the inherent α-relaxation. This is not a universal behavior, as mentioned in the Introduction since, for many systems, a negative shift or even no shift of the glass transition temperature relative to bulk is observed.[3,27]

At lower frequencies (higher temperatures) than the α-process, the above-mentioned S-process is observed for the confined system having a slower molecular dynamics. This points out a particular feature of the confined system.

This kind of S-process has been found for molecular guests interacting with the pore walls. Therefore, its molecular origin in the present system is associated with molecular fluctuations of the near surface Triton molecules. The simultaneous observation of an α-relaxation and an S-process allows classifying the dynamics of confined Triton molecules into two fractions: one liquid-like due to molecules close to the pore center with relaxation rates close to those of the bulk guest (although slightly inferior) and another due to molecules interacting with the pores with significantly hindered mobility. Two families of molecules with different mobilities were also observed in ibuprofen confined to the same kind of mesoporous matrix by multinuclear solid-state NMR.[31] It was observed by dielectric spectroscopy by some of us also for ibuprofen[28] and the liquid crystal mixture E7,[30] both impregnated in the same SBA porous matrix.

A VFTH equation was fitted to the temperature dependence of the relaxation times of this S-process, allowing estimating a glass transition temperature of 243.5 K, lying ~30 K above the glass transition estimated from dielectric data of the bulklike α-process of Triton/SBA. This increment of the glass transition of the surface process relative to the bulklike one is close to the temperature difference found by DSC between processes I and II (~20 K).

The interaction of guest Triton molecules with the pores may occur via hydrogen bonds between the OH terminal group of Triton and the surface silanol (Si−OH) groups present in the pore wall. Moreover, in the ibuprofen/SBA system and also in the liquid crystalline mixture E7 impregnated in the same porous host,[30] the S-process was the dominant one, as found here for confined Triton. This finding agrees with DSC results that showed a higher heat flow jump for process II, which was interpreted as a higher number of Triton molecules contributing to the glass transition observed at higher temperatures; this is also in agreement with a greater area below the TGA peak corresponding to the mass loss step detected at higher temperatures. From dielectric results, this conclusion is not so obvious since a higher intensity could arise from a preferential dipolar alignment instead of a higher number of relaxing dipoles. Nevertheless, the simultaneous analysis of the output of the three techniques seems to lead to the conclusion that indeed more Triton molecules are associated with the second glass transition step and that interact relatively strongly with the surface since it decomposes at higher temperatures relative to the bulklike material, as seen by the TGA analysis.

This strong interaction with the pore surface could, to some extent, destroy the locally structured domains conceptualized to exist in Triton[12] acting as an intermediate preordering step precluding the crystal formation. Indeed, this preordered structure was taken as one of the factors enabling nucleation/

crystal growth. It should be stressed that the relatively high fragility of neat Triton was taken as a factor that favored cold crystallization occurring very close to the glass transition.[12] This means that only a small increase in temperature above T_g increases the relaxation time to an extent that enables the mobility for molecules, which per se are already preordered, to rearrange in the crystalline network. Confined Triton has also a high fragility, but the material is prevented to crystallize either by the dimensions of the pore that make crystal growth impractical or by the disordered arrangement of molecules interacting with the pore wall, or even the concurrence of both factors. Although the macroscopical pore arrangement in SBA is ordered, it is an amorphous material. This means that, at the molecular level, the molecules are disorderly arranged. Therefore, adsorbed Triton molecules mimic the irregular landscape of the pore walls and, to some extent, act as a template for the inner molecules, impairing the buildup of an ordered pattern.

At even higher temperatures and lower frequencies than the S-process, an additional process emerges for Triton/SBA attributed to Maxwell−Wagner−Sillars (MWS) polarization. This phenomenon is related to the blocking of charge carriers at boundaries found in inhomogeneous materials, including nanoporous hosts,[61] which, in the present system, arises in Triton/SBA interfaces. The temperature dependence of this MWS process seems to be linear with $1/T$, over a relatively large interval including relaxation times obtained from both isochronal and isothermal analysis, and therefore, an apparent activation energy E_a can be estimated: $E_a = 81 \pm 2$ kJ·mol^{-1}. It is interesting to observe the similarity of the profile of relaxation times in the relaxation map between the $MWS_{Tr/SBA}$ and the S-processes. Therefore, it seems that the dynamic of the MWS in the Triton/SBA is mainly governed by the S-process This supports the assumption for the confined system that the interface giving rise to the MWS polarization is mainly due to adsorbed molecules/SBA rather than bulklike molecules/SBA.

5. CONCLUSIONS

The strong crystallization tendency of the glass-former Triton X-100 is shown by DSC, which evidences that, even at high heating rates, such as 30 K·min^{-1}, bulk Triton crystallizes.

Inclusion of Triton X-100 into a mesoporous silica-based matrix (SBA-15) with a 5.7 nm pore diameter was used as a means to surpass crystallization. The evaluation of the loading efficiency was provided first by ATR-FTIR and further by TGA, giving a loading degree of around 50% (wt).

For Triton/SBA, powder X-ray diffraction patterns only present the amorphous halo under any thermal treatment, while Bragg peaks emerge due to crystallization for bulk Triton X-100 upon heating from an initial quenched amorphous state at 173 K, followed by melting; this proves that the molecular guest exists in a thermally stable amorphous form when confined to the SBA-15 matrix. The long-term stability was confirmed by calorimetric and dielectric measurements 24 months after inclusion.

In the dielectric spectra of confined Triton, in addition to the multiple amorphous bulklike relaxation processes, an S-process assigned to the Triton molecules interacting with the internal pore wall is detected and an MWS as well. These results demonstrate the existence of two families of molecules with different molecular mobilities: (i) one family, due to molecules absorbed at the walls with significantly hindered mobility, whose calorimetric glass transition temperature is ∼20 K higher than T_{g,am_bulk}, and (ii) another family due to the confined liquid consisting of molecules located more in the center of the pores only slightly slowed down relative to bulk amorphous, the respective T_g being ∼3 K higher than the T_{g,am_bulk}.

The evidence of the two molecular families was also given by TGA that shows a two-step profile. The analysis of the derivative of the TGA plot allows concluding that a significant number of molecules are adsorbed, giving rise to a pronounced glass transition process that was detected by DSC besides the bulklike glass transition. The unambiguous detection under conventional DSC conditions of two well-resolved heat flux discontinuities associated with the glass transitions of each family of different molecular mobility reinforces the character of Triton X-100 as a model compound to illustrate such fundamental effects of the condensed matter physics.

In addition, inclusion in a silica-based nanostructured matrix of 5.7 nm in pore diameter revealed to be a good strategy to suppress crystallization in Triton X-100.

AUTHOR INFORMATION

Corresponding Authors

*E-mail: natalia.correia@univ-lille1.fr.
*E-mail: madalena.dionisio@fct.unl.pt.

Notes

The authors declare no competing financial interest.

ACKNOWLEDGMENTS

The authors acknowledge Professor J. C. Sotomayor (Requimte, FCT/UNL, Portugal) for the suggestion to investigate Triton X-100. Financial support for this work was provided through contract PEst-C/EQB/LA0006/2011 and the project PTDC/CTM/098979/2008 implemented within the framework of the Programme "Promover a Produção Científica, o Desenvolvimento Tecnológico e a Inovação 002: Investigação Científica e Tecnológica (3599-PPCDTI)" financed by Fundação para a Ciência e Tecnologia (FCT), IP.

REFERENCES

(1) Schick, C. Glass Transition under Confinement-What Can Be Learned from Calorimetry. *Eur. Phys. J.: Spec. Top.* **2010**, *189*, 3−36.
(2) *Proceedings of the 4th International Workshop on Dynamics in Confinement*, Grenoble, France, March 3−5, 2010; Institut Laue-Langevin: Grenoble, France, 2010.
(3) Kremer, F.; Huwe, A.; Schönhals, A.; Różański, S. A. Molecular Dynamics in Confining Space. In *Broadband Dielectric Spectroscopy*; Kremer, F., Schönhals, A., Eds.; Springer-Verlag: Berlin, 2003; Chapter 6.
(4) Hartmann, L.; Fukao, K.; Kremer, F. Molecular Dynamics in Thin Polymer Films. In *Broadband Dielectric Spectroscopy*; Kremer, F., Schönhals, A., Eds.; Springer-Verlag: Berlin, 2003; Chapter 11.
(5) Napolitano, S.; Rotella, C.; Wübbenhorst, M. Can Thickness and Interfacial Interactions Univocally Determine the Behavior of Polymers Confined at the Nanoscale? *ACS Macro Lett.* **2012**, *1*, 1189−1193.
(6) Kawaguchi, D.; Tanaka, K.; Kajiyama, T.; Takahara, A.; Tasaki, S. Mobility Gradient in Surface Region of Monodisperse Polystyrene Films. *Macromolecules* **2003**, *36*, 1235−1240.
(7) Inoue, R.; Kawashima, K.; Matsui, K.; Kanaya, T.; Nishida, K.; Matsuba, G.; Hino, M. Distributions of Glass-Transition Temperature and Thermal Expansivity in Multilayered Polystyrene Thin Films Studied by Neutron Reflectivity. *Phys. Rev. E* **2011**, *83*, 021801.
(8) Park, J.-Y.; Mckenna, G. B. Size and Confinement Effects on the Glass Transition Behavior of Polystyrene/*o*-terphenyl Polymer Solutions. *Phys. Rev. B* **2000**, *61*, 6667−6676.

(9) Trofymluk, O.; Levchenko, A. A.; Navrotsky, A. Interfacial Effects on Vitrification of Confined Glass-Forming Liquids. *J. Chem. Phys.* **2005**, *123*, 194509.
(10) Zheng, W.; Simon, S. L. Confinement Effects on the Glass Transition of Hydrogen Bonded Liquids. *J. Chem. Phys.* **2007**, *127*, 194501.
(11) Rengarajan, G. T.; Enke, D.; Steinhart, M.; Beiner, M. Stabilization of the Amorphous State of Pharmaceuticals in Nanopores. *J. Mater. Sci.* **2008**, *18*, 2537−2539 (ESI; Fig. S3).
(12) Merino, E. G.; Rodrigues, C.; Teresa Viciosa, M.; Melo, C.; Sotomayor, J.; Dionísio, M.; Correia, N. T. Phase Transformations Undergone by Triton X-100 Probed by Differential Scanning Calorimetry and Dielectric Relaxation Spectroscopy. *J. Phys. Chem. B* **2011**, *115*, 12336−12347.
(13) Merino, E. G.; Danéde, F.; Derrollez, P.; Dias, C. J.; Viciosa, M. T.; Correia, N. T.; Dionísio, M. Investigating the Influence of Morphology in the Dynamical Behavior of Semicrystalline Triton X-100: Insights in the Detection/Nondetection of the α'-Process. *J. Phys. Chem. B* **2013**, *117*, 9793−9805.
(14) Viciosa, M. T.; Correia, N. T.; Salmerón Sanchez, M.; Gómez Ribelles, J. L.; Dionísio, M. Molecular Dynamics of Ethylene Glycol Dimethacrylate Glass Former: Influence of Different Crystallization Pathways. *J. Phys. Chem. B* **2009**, *113*, 14196−14208.
(15) Viciosa, M. T.; Brás, A. R.; Gómez Ribelles, J. L.; Dionisio, M. Polymerization Effects on Molecular Dynamics of *n*-Ethylene Glycol Dimethacrylates Followed by Dielectric Relaxation Spectroscopy. *Eur. Polym. J.* **2008**, *44*, 155−170.
(16) Beiner, M.; Rengarajan, G. T.; Pankaj, S.; Enke, D.; Steinhart, M. Manipulating the Crystalline State of Pharmaceuticals by Nanoconfinement. *Nano Lett.* **2007**, *7*, 1381−1385.
(17) Rengarajan, G. T.; Enke, D.; Steinhart, M.; Beiner, M. Size-Dependent Growth of Polymorphs in Nanopores and Ostwald's Step Rule of Stages. *Phys. Chem. Chem. Phys.* **2011**, *13*, 21367−21374.
(18) Jackson, C. L.; McKenna, G. B. Vitrification and Crystallization of Organic Liquids Confined to Nanoscale Pores. *Chem. Mater.* **1996**, *8*, 2128−2137.
(19) Bergman, R.; Swenson, J. Dynamics of Supercooled Water in Confined Geometry. *Nature* **2000**, *403*, 283−286.
(20) Konno, T.; Kinuno, K.; Kataoka, K. Physical and Chemical Changes of Medicinals in Mixtures with Adsorbents in the Solid State. I. Effect of Vapor Pressure of the Medicinals on Changes in Crystalline Properties. *Chem. Pharm. Bull.* **1986**, *34*, 301−307.
(21) Ajayan, P. M.; Iijima, S. Capillarity-Induced Filling of Carbon Nanotubes. *Nature* **1993**, *361*, 333−334.
(22) Prasad, R.; Lele, S. Stabilization of the Amorphous Phase Inside Carbon Nanotubes: Solidification in a Constrained Geometry. *Philos. Mag. Lett.* **1994**, *70*, 357−361.
(23) Leys, J.; Sinha, G.; Glorieux, C.; Thoen, J. Influence of Nanosized Confinements on 4-*n*-decyl-4′-cyanobiphenyl (10CB): A Broadband Dielectric Study. *Phys. Rev. E* **2005**, *71*, 051709.
(24) Koppensteiner, J.; Schranz, W.; Carpenter, M. A. Revealing the Pure Confinement Effect in Glass-Forming Liquids by Dynamic Mechanical Analysis. *Phys. Rev. B* **2010**, *81*, 024202.
(25) Kranbuehl, D.; Knowles, R.; Hossain, A.; Hurt, M. Modelling the Effects of Confinement on the Glass Transition Temperature and Segmental Mobility. *J. Phys.: Condens. Matter.* **2003**, *15*, S1019−S1029.
(26) Iacob, C.; Sangoro, J. R.; Papadopoulos, P.; Schubert, T.; Naumov, S.; Valiullin, R.; Kärger, J.; Kremer, F. Charge Transport and Diffusion of Ionic Liquids in Nanoporous Silica Membranes. *Phys. Chem. Chem. Phys.* **2010**, *12*, 13798−13803.
(27) Richert, R. Dynamics of Nanoconfined Supercooled Liquids. *Annu. Rev. Phys. Chem.* **2011**, *62*, 65−84.
(28) Brás, A. R.; Merino, E. G.; Neves, P. D.; Fonseca, I. M.; Dionísio, M.; Schönhals, A.; Correia, N. T. Amorphous Ibuprofen Confined in Nanostructured Silica Materials: A Dynamical Approach. *J. Phys. Chem. C* **2011**, *115*, 4616−4623.
(29) Arndt, M.; Stannarius, R.; Gorbatschow, W.; Kremer, F. Dielectric Investigations of the Dynamic Glass Transition in Nanopores. *Phys Rev. E* **1996**, *54*, 5377−5390.
(30) Brás, A. R.; Frunza, S.; Guerreiro, L.; Fonseca, I. M.; Corma, A.; Frunza, L.; Dionísio, M.; Schönhals, A. Molecular Mobility of Nematic E7 Confined to Molecular Sieves with a Low Filling Degree. *J. Chem. Phys.* **2010**, *132*, 224508.
(31) Izquierdo-Barba, I.; Sousa, E.; Doadrio, J. C.; Doadrio, A. L.; Pariente, J. P.; Martínez, A.; Babonneau, F.; Vallet-Regí, M. Influence of Mesoporous Structure Type on the Controlled Delivery of Drugs: Release of Ibuprofen from MCM-48, SBA-15 and Functionalized SBA-15. *J. Sol−Gel Sci. Technol.* **2009**, *50*, 421−429.
(32) Buntkowsky, G.; H Breitzke, H.; Adamczyk, A.; Roelofs, F.; Emmler, T.; Gedat, E.; Grünberg, B.; Xu, Y.; Limbach, H.-H.; Shenderovich, I.; et al. Structural and Dynamical Properties of Guest Molecules Confined in Mesoporous Silica Materials Revealed by NMR. *Phys. Chem. Chem. Phys.* **2007**, *9*, 4843−4853.
(33) Ruiz-Hitzky, E., Ariga, K., Lvov, Y. M., Eds. *Bio-inorganic Hybrid Nanomaterials: Strategies, Syntheses, Characterization and Applications*; Wiley-VCH: Weinheim, Germany, 2008.
(34) Gao, L.; Wang, Y.; Wang, J.; Huang, L.; Shi, L.; Fan, X.; Zou, Z.; Yu, T.; Zhu, M.; Li, Z. A Novel Zn^{II}-Sensitive Fluorescent Chemosensor Assembled within Aminopropyl-Functionalized Mesoporous SBA-15. *Inorg. Chem.* **2006**, *45*, 6844−6850.
(35) Barrett, E. P.; Joyner, L. G.; Halenda, P. P. The Determination of Pore Volume and Area Distributions in Porous Substances. I. Computations From Nitrogen Isotherms. *J. Am. Chem. Soc.* **1951**, *73*, 373−380.
(36) Derollez, P.; Dudognon, E.; Affouard, F.; Danède, F.; Correia, N. T.; Descamps, M. Ab Initio Structure Determination of Phase II of Racemic Ibuprofen by X-ray Powder Diffraction. *Acta Crystallogr., Sect. B* **2010**, *66*, 76−80.
(37) Menczel, J. D., Prime, R. B., Eds. *Thermal Analysis of Polymers, Fundamentals and Applications*; John While & Sons, Inc.: Hoboken, NJ, 2009.
(38) Schönhals, A.; Kremer, F. Analysis of Dielectric Spectra. In *Broadband Dielectric Spectroscopy*; Kremer, F., Schönhals, A., Eds.; Springer Verlag: Berlin, 2003; Chapter 3.
(39) Boersma, A.; Van Turnhout, J.; Wübbenhorst, M. Dielectric Characterization of a Thermotropic Liquid Crystalline Copolyesteramide: 1. Relaxation Peak Assignment. *Macromolecules* **1998**, *31*, 7453−7460.
(40) Schröter, K.; Unger, R.; Reissig, S.; Garwe, F.; Kahle, S.; Beiner, M.; Donth, E. Dielectric Spectroscopy in the $\alpha\beta$ Splitting Region of Glass Transition in Poly(ethyl methacrylate) and Poly(*n*-butyl methacrylate): Different Evaluation Methods and Experimental Conditions. *Macromolecules* **1998**, *31*, 8966−8972.
(41) Vogel, H. The Temperature Dependence Law of the Viscosity of Fluids. *Phys. Z.* **1921**, *22*, 645−646.
(42) Fulcher, G. S. Analysis of Recent Measurements of the Viscosity of Glasses. *J. Am. Ceram. Soc.* **1925**, *8*, 339−355.
(43) Tammann, G.; Hesse, W. The Dependancy of Viscosity on Temperature in Hypothermic Liquids. *Z. Anorg. Allg. Chem.* **1926**, *156*, 245−257.
(44) Barnett, S. M.; Dracheva, S.; Hendler, R. W.; Levin, I. W. Lipid-Induced Conformational Changes of an Integral Membrane Protein: An Infrared Spectroscopic Study of the Effects of Triton X-100 Treatment on the Purple Membrane of Halobacterium Halobium ET1001. *Biochemistry* **1996**, *35*, 4558−4567.
(45) Yoshihara, T.; Tadokoro, H.; Murahashi, S. Normal Vibrations of the Polymer Molecules of Helical Conformation. IV. Polyethylene Oxide and Polyethylene-d_4 Oxide. *J. Chem. Phys.* **1964**, *41*, 2902−2911.
(46) Tropecêlo, A. I.; Casimiro, M. H.; Fonseca, I. M.; Ramos, A. M.; Vital, J.; Castanheiro, J. E. Esterification of Free Fatty Acids to Biodiesel over Heteropolyacids Immobilized on Mesoporous Silica. *Appl. Catal., A* **2010**, *390*, 183−189.
(47) Mellaerts, R.; Jammaer, J. A. G.; Van Speybroeck, M.; Chen, H.; Van Humbeeck, J.; Augustijns, P.; Van den Mooter, G.; Martens, J. A. Physical State of Poorly Water Soluble Therapeutic Molecules Loaded into SBA-15 Ordered Mesoporous Silica Carriers: A Case Study with Itraconazole and Ibuprofen. *Langmuir* **2008**, *24*, 8651−8659.

(48) Shen, S. C.; Ng, W. K.; Chia, L.; Dong, Y. C.; Tan, R. B. Stabilized Amorphous State of Ibuprofen by Co-spray Drying with Mesoporous SBA-15 to Enhance Dissolution Properties. *J. Pharm. Sci.* **2010**, *99*, 1997−2007.
(49) Simon, S. L.; Park, J.-Y.; McKenna, G. B. Enthalpy Recovery of a Glass-Forming Liquid Constrained in a Nanoporous Matrix: Negative Pressure Effects. *Eur. Phys. J. E* **2002**, *8*, 209−216.
(50) Boucher, V. M.; Cangialosi, D.; Alegría, A.; Colmenero, J. Enthalpy Recovery in Nanometer to Micrometer Thick Polystyrene Films. *Macromolecules* **2012**, *45*, 5296−5306.
(51) During revision of the manuscript, a DSC was scanned once more and the two transitions persist in the registered thermogram without any sign of crystallization/melting.
(52) Arndt, M.; Stannarius, R.; Groothues, H.; Hempel, E.; Kremer, F. Length Scale of Cooperativity in the Dynamic Glass Transition. *Phys. Rev. Lett.* **1997**, *79*, 2077−2080.
(53) Frunza, L.; Frunza, S.; Kosslick, H.; Schönhals, A. Phase Behavior and Molecular Mobility of *n*-Octylcyanobiphenyl Confined to Molecular Sieves: Dependence on the Pore Size. *Phys. Rev. E* **2008**, *78*, 051701.
(54) Schüller, J.; Mel'nichenko, Y. B.; Richert, R.; Fischer, E. W. Dielectric Studies of the Glass Transition in Porous Media. *Phys. Rev. Lett.* **1994**, *73*, 2224−2227.
(55) Hartmann, L.; Kremer, F.; Pouret, P.; Léger, L. Molecular Dynamics in Grafted Layers of Poly(dimethylsiloxane). *J. Chem. Phys.* **2003**, *118*, 6052−6058.
(56) Smith, I. K.; Andrews, S. R.; Williams, G.; Holmes, P. A. Bulk Thermal Polymerisation of Diethylene Glycol Bis(allyl carbonate) as Studied by Dielectric Relaxation Spectroscopy. *J. Mater. Chem.* **1997**, *7*, 203−209.
(57) Viciosa, M. T.; Rodrigues, C.; Fernandez, S.; Matos, I.; Marques, M. M.; Duarte, M. T.; Mano, J. F.; Dionísio, M. Dielectric and Thermal Characterization of Low Density Ethylene/10-Undecen-1-ol Copolymers Prepared with Nickel Catalysts. *J. Polym. Sci., Part B: Polym. Phys.* **2007**, *45*, 2802−2812.
(58) Van Turnhout, J.; Wübbenhorst, M. Analysis of Complex Dielectric Spectra. II: Evaluation of the Activation Energy Landscape by Differential Sampling. *J. Non-Cryst. Solids* **2002**, *305*, 50−58.
(59) Böhmer, R.; Ngai, K. L.; Angell, C. A.; Plazek, D. J. Nonexponential Relaxations in Strong and Fragile Glass Formers. *J. Chem. Phys.* **1993**, *99*, 4201−4209.
(60) Moynihan, C. T.; Macedo, P. B.; Montrose, C. J.; Gupta, P. K.; DeBolt, M. A.; Dill, J. F.; Dom, B. E.; Drake, P. W.; Esteal, A. J.; Elterman, P. B.; et al. Structural Relaxation in Vitreous Materials. *Ann. N. Y. Acad. Sci.* **1976**, *279*, 15−35.
(61) Steeman, P. A. M.; van Turnhout, J. Dielectric Properties in Inhomogeneous Media. In *Broadband Dielectric Spectroscopy*; Kremer, F., Schönhals, A., Eds.; Springer Verlag: Berlin, 2003, Chapter 13.